


Relative navigation technique with constrained GNSS data for formation-flying CubeSat mission, CANYVAL-C

Eunji Lee | Jihae Son | Sang-Young Park 

Department of Astronomy, Yonsei University, 50 Yonsei-ro Seodaemun-gu, Seoul 03722, Republic of Korea

Correspondence

Sang-Young Park, Department of Astronomy, Yonsei University, 50 Yonsei-ro Seodaemun-gu, Seoul 03722, Republic of Korea

Email: spark624@yonsei.ac.kr

Funding information

National Research Foundation of Korea, Grant/Award Number: NRF-2017M1A3A3A06085349

Abstract

This study introduces and verifies a relative navigation technique for two CubeSats in formation flying as part of the CANYVAL-C mission. Because the mission requires precision and robustness subject to restricted computational complexity, the technique employs an Extended Kalman Filter (EKF) and raw GNSS data to achieve relative navigation. The relative navigation technique is composed of two parts: parameter-tuning using an Adaptive Kalman Filter (AKF) in a ground station, and the application of the adaptively determined parameters to allow onboard EKF. Based on Hardware-in-the-Loop Simulations (HILS), the relative positioning error of the EKF with adaptively determined parameters ranged from 10 to 20 cm on each axis (3σ) and satisfied the mission requirement of 1 m. The simulations confirm that the technique yields reliable relative navigation and a realistic error covariance without imposing a computational burden on the CubeSat, as well as reduces the time required for parameter tuning.

KEYWORDS

cubesat, GNSS data, relative navigation

1 | INTRODUCTION

CubeSat, a standardized satellite with a cube unit of 10 cm, is cost- and time-efficient because of its small size and standardization in terms of aspects such as structure and interface. It has been employed in experimental and challenging flying missions: demonstrating a deployable telescope with FalconSAT-7 (Andersen et al., 2012); exploring deep space with Mars Cube One (Klesh et al., 2018); and exploring a galactic halo in the Milky Way galaxy with HaloSat (Kaaret et al., 2019).

Furthermore, the use of a formation or constellation of multiple CubeSats has been proposed as an alternative to huge space missions like the Dynamic Ionosphere CubeSat Experiment (DICE), in which two 1.5U CubeSats investigated the ionospheric storm enhanced density (Fish et al., 2014), as well as the SeaHawk, which observed changes

in ocean color using two 3U CubeSats (Morrison et al., 2016). To succeed in a formation-flying mission, a precise Guidance, Navigation, and Control (GNC) algorithm including relative navigation is necessary. Several CubeSat missions have employed precise, relative navigation algorithms.

The CubeSat Proximity Operations Demonstration (COPD) was a mission composed of two 3U CubeSats used to verify rendezvous, proximity, and docking operations. The Rendezvous-Proximity Operations (RPO) GNC subsystem that was implemented in a separate onboard processor estimated the absolute inertial state of the host CubeSat and the relative state of the other CubeSat by using an Extended Kalman Filter (EKF) as the real-time estimation algorithm.

It employs a GPS Intersatellite Link (ISL) range, with optical sensor measurements as observation data, and a

This is an open access article under the terms of the [Creative Commons Attribution-NonCommercial-NoDerivs](https://creativecommons.org/licenses/by-nc-nd/4.0/) License, which permits use and distribution in any medium, provided the original work is properly cited, the use is non-commercial and no modifications or adaptations are made.

© 2021 The Authors. *NAVIGATION* published by Wiley Periodicals LLC on behalf of Institute of Navigation.

force model that contains an 8×8 spherical harmonic gravity field (EGM2008 model), atmospheric drag (a modified Harris Priester atmospheric density model), and third-body perturbations (lunar and solar). The GNC algorithm was tested through Software-in-the-Loop and Hardware-in-the-Loop Simulations (HILS), resulting in the relative navigation accuracy being several tens of centimeters during the mid-range formation reconfiguration maneuver (Roscoe et al., 2018).

CanX-4 and CanX-5 were a pair of two identical 8U CubeSats that aimed to demonstrate autonomous formation control (Bonin et al., 2015). The pair used two navigation algorithms that both employed EKF to implement coarse and relative navigation. The coarse navigation took the absolute orbit solution provided by the GPS receiver and smoothed it using orbital dynamics, including the 6×6 gravity field. The relative navigation employed a Differential GPS (DGPS) method with raw GPS data and the same dynamics. Both CubeSats controlled the GPS antenna to ensure that the zenith received as many common GPS signals as possible, and an additional attitude control was conducted to minimize the effect of the slewing of GPS satellites (Johnston-Lemke & Zee, 2010). It achieved a relative accuracy < 10 cm that degraded to several meters during maneuvering (Kahr et al., 2018).

The CubeSat Astronomy by NASA and Yonsei using the Virtual Telescope Alignment (CANYVAL) project was designed to demonstrate inertial alignment, a key technique of the virtual telescope. It consisted of two satellites that functioned as a lens and detector, respectively (Calhoun et al., 2018; Park et al., 2014; Shah et al., 2013). The first experimental mission, CANYVAL-X (CANYVAL-eXperiment), was comprised of two CubeSats (1U and 2U) that were launched in 2018. It was designed to maintain a relative distance and aligned with respect to the Sun based on a vision alignment system (Park et al., 2016).

CANYVAL-Coronagraph (CANYVAL-C), the follow-up mission of CANYVAL-X, was also comprised of 1U and 2U CubeSats. The 1U CubeSat captured images of the solar corona during the 2U CubeSat occults of the solar sphere, and they were aligned with respect to the Sun (Kim et al., 2019). CANYVAL-C employed EKF using raw GNSS data for real-time relative navigation between the two CubeSats necessary to satisfy the mission requirements subject to imposed constraints.

Although EKF is a simple and efficient estimation algorithm, it is necessary to empirically tune the dynamic and measurement noise covariances that significantly influence estimation performance. Parameter tuning is complicated, especially in space missions because the actual circumstances cannot be known before launch. Therefore, various adaptive algorithms to be employed in space missions have been proposed to estimate the covariances.

In Busse et al. (2003), an adaptive method of maximum likelihood estimation was implemented in a formation-flying mission to achieve robust and precise relative navigation accuracy by compensating for systematic uncertainty. The research demonstrated a relative position accuracy of 2 cm by HILS, while improper parameters led to a divergence of estimation.

He et al. (2012) improved an adaptive Sage filter by adopting a weighted average quadratic form into covariance matching. The weight was defined to be larger with a shorter distance or smaller variance. This allowed the estimation of the covariances based on consideration of the precision and correlation of the residuals and states. The algorithm was verified based on two cases: a maneuvering Geostationary (GEO) satellite and an aircraft. As a result, the proposed algorithm showed more precise and robust performance, especially with disturbances.

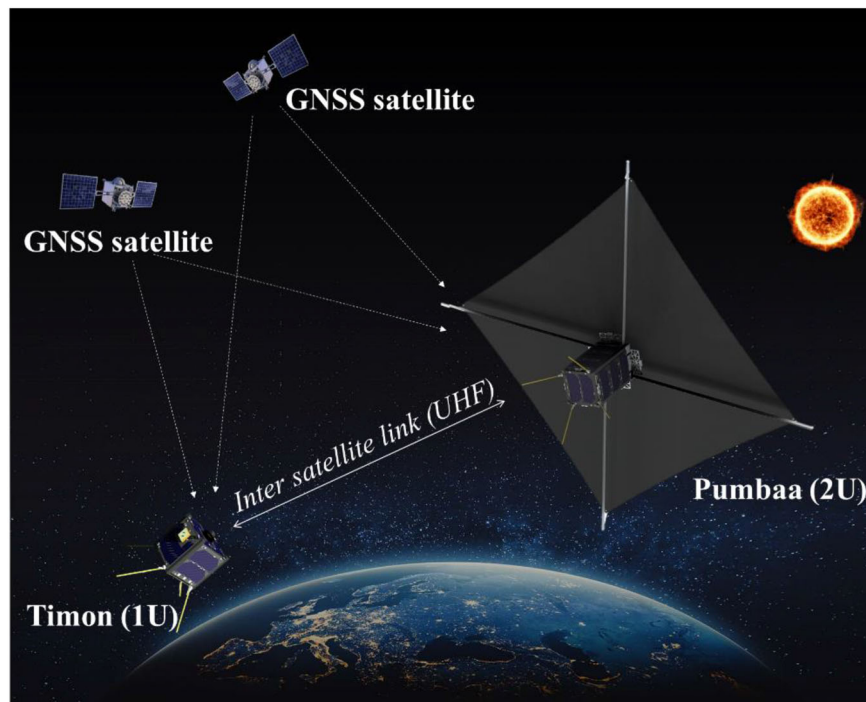
Another study (Karlgard & Schaub, 2011) suggested an adaptive nonlinear filter based on Huber's maximum likelihood estimation and modified the Myers–Tapley covariance matching algorithm. It was applied to the six-degrees-of-freedom elliptical orbit rendezvous and docking problem, and it provided superior performance in non-Gaussian noise cases. The computational time, however, increased two- or even four-fold, which is improper for real-time applications with limited processing performance.

An adaptive EKF that can be implemented on a processor with limited capability was proposed by Xiao et al. (2018). The adaptive process decreased the positioning error by 20% even with simple dynamics and only slightly increased the computational burden. However, although the process determined the measurement noise covariance based on the carrier-to-noise ratio, the dynamic noise covariance remained undetermined.

In this study, a method and operational technique using an EKF and modified AKF for precise and robust relative navigation subject to the uncertainty and processing limitation of the CANYVAL-C mission was proposed. Considering the limited onboard processing capabilities and necessity of real-time navigation for the CANYVAL-C mission, the technique consisted of two steps to minimize the computational burden: a) an adaptive algorithm would determine the measurement and dynamic noise covariance in the ground station, and b) the adaptively determined parameters would be uploaded to the CubeSats and applied to achieve onboard EKF.

Conducting HILS based on the CANYVAL-C mission scenarios, the proposed technique was verified and confirmed in improving the reliability of the relative navigation without increasing the computational burden of the CubeSat's onboard computer. The adaptive process reduced the time and effort required to identify

FIGURE 1 Concept of CANYVAL-C
[Color figure can be viewed in the online issue, which is available at wileyonlinelibrary.com and www.ion.org]



proper tuning parameters by robustly determining them, regardless of the initial guess. In addition, the adaptively determined parameters emulated the real environment and compensated for system errors. The estimation accuracy can be assessed by the error covariance matrix which provides a realistic error boundary, as emphasized in Busse et al. (2003). The technique will be applied to practical operations after the launch of CANYVAL-C in early 2021.

This paper consists of five sections. Section 2 briefly introduces the CANYVAL-C mission and addresses the requirements and constraints for relative navigation. Section 3 mathematically describes the modified AKF and defines the relative navigation problem of CANYVAL-C. The circumstances and results of HILS used to verify the proposed technique are presented in Section 4. Section 5 presents the conclusions drawn in the study.

2 | CANYVAL-C

2.1 | Mission overview

CANYVAL-C is a mission set out to acquire solar coronagraphs using two CubeSats that are precisely aligned with respect to the Sun. The 2U CubeSat, Pumbaa, extends an occulter to block the solar sphere and allow the occurrence of the corona, while the CubeSat with a size of 1U, Timon, has a camera and serves as a detector (Figure 1).

CANYVAL-C can prove the possibility of implementing a virtual telescope and verify key techniques, such as inertial alignment and precise relative orbit maintenance (Kim et al., 2019). The orbit is a Sun-synchronous orbit with an altitude of 525 km, whereas the Proba-3, which has a simi-

lar concept, will be launched in a Highly Eccentric Orbit (HEO) with a 20 h orbital period (Llorente et al., 2013). Low Earth Orbits (LEO) are more affected by the gravity gradient disturbances compared to HEO, so a sophisticated GNC algorithm is required for the CANYVAL-C mission.

The mission consists of three phases: Launch and Early Orbit Phase (LEOP), Drift Recovery and Station Keeping Phase (DRSKP), and the Autonomous Formation-Flying Phase (AFFP). In the LEOP, both CubeSats deploy their antennas, stabilize spin, and commission each hardware component. In the DRSKP, Pumbaa conducts orbit maneuvers to prevent divergence and maintain a maximum distance of 10 km between the CubeSats. In the AFFP, the two CubeSats are aligned with respect to the Sun based on the precise relative position obtained by a relative navigation algorithm using the DGPS method; they acquire the coronagraphs and automatically maintain the formation.

The DRSKP and AFFP include several operation modes: commission, normal, communication, emergency, control, and mission mode. The GNSS receiver is turned on and initialized in the commission mode, the CubeSats stand by in the normal mode, and communication between the CubeSats and the ground station is conducted in the communication mode. The CubeSats autonomously enter the emergency mode based on status.

In the control mode, the propulsion system and Differential Air Drag Control (DADC) are employed. The propulsion system is composed of four cold gas thruster nozzles and provides a 1 mN impulse with a pulse width of 10 ms. In the DRSKP, it performs maneuvers to maintain a relative distance under 10 km. In the AFFP, it conducts the maneuvers for the Rendezvous (RDV) and Inertial

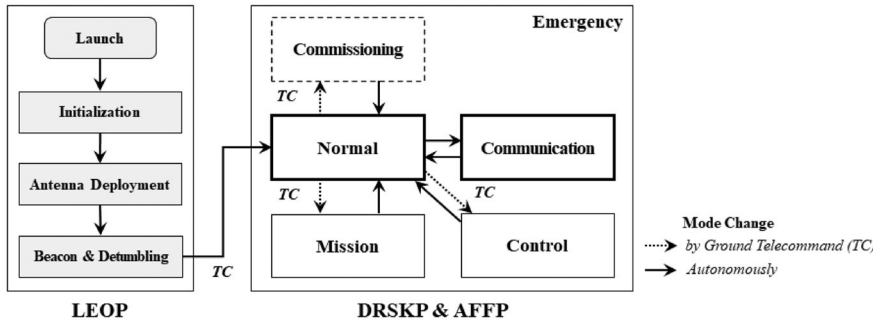


FIGURE 2 Structure of phases and modes for CANYVAL-C operation (Kim et al., 2019)

TABLE 1 Navigation mode and required accuracy along mission phases and modes of CANYVAL-C

Operation phase	Operation mode	Navigation mode	Navigation requirement	
			Absolute (3σ)	Relative (3σ)
Launch and Early Orbit Phase (LEOP)	-	-	-	-
-	Emergency	-	-	-
Drift Recovery and Station Keeping Phase (DRSKP)	Commission	Orbit prediction	-	2 km (3D)
	Normal			
	Communication			
	Control			
Autonomous Formation-Flying Phase (AFFP)	Normal	Coarse	50 m (3D)	60 m (1D)
	Commission			
	Communication			
	Control	Fine		1 m (1D)
	Mission			

Alignment Hold (IAH) to maintain the relative distance between the CubeSats and alignment of the CubeSats with respect to the Sun (Kim et al., 2019). The DADC, which induces the relative acceleration of the two CubeSats using the differential atmospheric drag forces between them by changing the effective cross section area (Leonard et al., 1989), is autonomously executed before and after the IAH to maintain the formation and distance between the CubeSats within 10 km. In mission mode, the camera on Timon acquires coronagraphs based on the IAH.

Figure 2 presents the structure of the phases and modes for operation. The bold arrows indicate autonomous mode switching by monitoring the system status, and is applied to basic modes including normal, communication, and emergency. Note that the CubeSat enters emergency mode if the status is determined unhealthy. The dashed arrows indicate mode change via ground commands, executed in commission, control, and mission modes (Kim et al., 2019).

With the use of numerical analysis, the requirements to obtain a proper coronagraph were determined. The CubeSats should maintain a relative distance of 40 ± 5 m (3σ) and align in a line by an angle under 7.5° with respect to the Sun (Kim et al., 2019). Note that Pumbaa controls orbit, keeping the location within a cone that has a radius and angle corresponding to the requirements, and heads from Timon to the Sun.

2.2 | Requirements and constraints on navigation

Relative navigation is comprised of three navigation modes: orbit prediction, coarse, and fine. Each navigation mode using separate navigation methods is employed to achieve the different requirements of each operation mode. In LEOP and the emergency mode of all phases, relative navigation is not executed. For drift recovery, the relative states are computed based on the predicted orbit by the ground station, that is, the orbit prediction mode.

Relative position uncertainty is required to be maintained under 2 km (3σ) in 3D. When the CubeSats execute DADC, the relative navigation enters the coarse mode and employs the subtraction of the orbit solutions, computed by each GNSS receiver as the relative states, to achieve the relative position accuracy of 60 m (3σ) on each axis. The fine mode based on the DGPS technique is started in the RDV and IAH that require relative uncertainties less than 1 m (3σ) along each axis.

Table 1 summarizes the navigation mode and required accuracy for the absolute and relative position with respect to the operation modes and phases. Note that strict requirements are only for relative states, and the requirement for

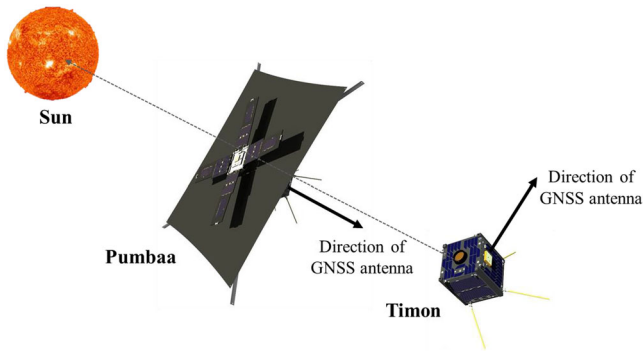


FIGURE 3 GNSS antenna arrangement of two CubeSats in the Inertial Alignment Hold (IAH) mode [Color figure can be viewed in the online issue, which is available at wileyonlinelibrary.com and www.ion.org]

the absolute position is set to 50 m in three-dimensions 3D (3σ) in both coarse and fine modes.

There are several constraints associated with the design of a navigation system owing to hardware limitations and mission characteristics. The GNSS antennas of Timon and Pumbaa are arranged orthogonally to each other during the IAH (Figure 3), whereas another formation-flying mission, CanX-4/5, controlled the attitude to point the zenith to acquire common signals as much as possible (Kahr et al., 2018). The arrangement derived from a limitation of the CubeSat design almost halved the number of common GNSS signals compared to the case facing the same direction. Figure 4 is an example of the comparison during one orbit period. To overcome this limitation and ensure that an adequate signal is received from at least four satellites

for precise, relative navigation, CANYVAL-C will employ both GPS and GLONASS signals.

CANYVAL-C has a GNSS antenna and receiver for the reception and processing of the signal in L1 frequency. The antenna TW1421 (Tallysman) had a gain of 28 dB, and the receiver OEM719 (NovAtel) received the signal with a frequency of 1 Hz and provided an orbit solution with a 1.6 m position accuracy. Although this is sufficient for the coarse mode, a more refined algorithm is required for fine mode.

The CubeSat, however, was equipped with a single processor that operates at a clock speed of 400 MHz (Cortex A9, Nara Space Tech.) wherein all the tasks including real-time relative navigation were executed (Kim et al., 2019). A light estimator is required to minimize the computational burden of relative navigation, and CANYVAL-C employed a simple EKF excluding terms with perturbation forces. In total, the relative navigation process required 0.75 s; 0.6 s are needed for ISL to transmit GNSS data (sizes of 550 bytes) using ultrahigh frequencies at the speed of 9600 bits per second, while 0.1 s are needed for data parsing, and 0.05 s is needed for EKF.

CANYVAL-C generated electrical power through the solar panels attached to a small surface. Because the power was not sufficient, the GNSS receiver was periodically turned off. The on-off periods were determined based on the system design and analysis.

In coarse navigation mode, Timon turned on the receiver for only for 20 min during four orbital periods, and Pumbaa turned on the receiver for 30 min during an orbital period. When the ground command for starting the fine navigation mode occurred, Timon and Pumbaa would

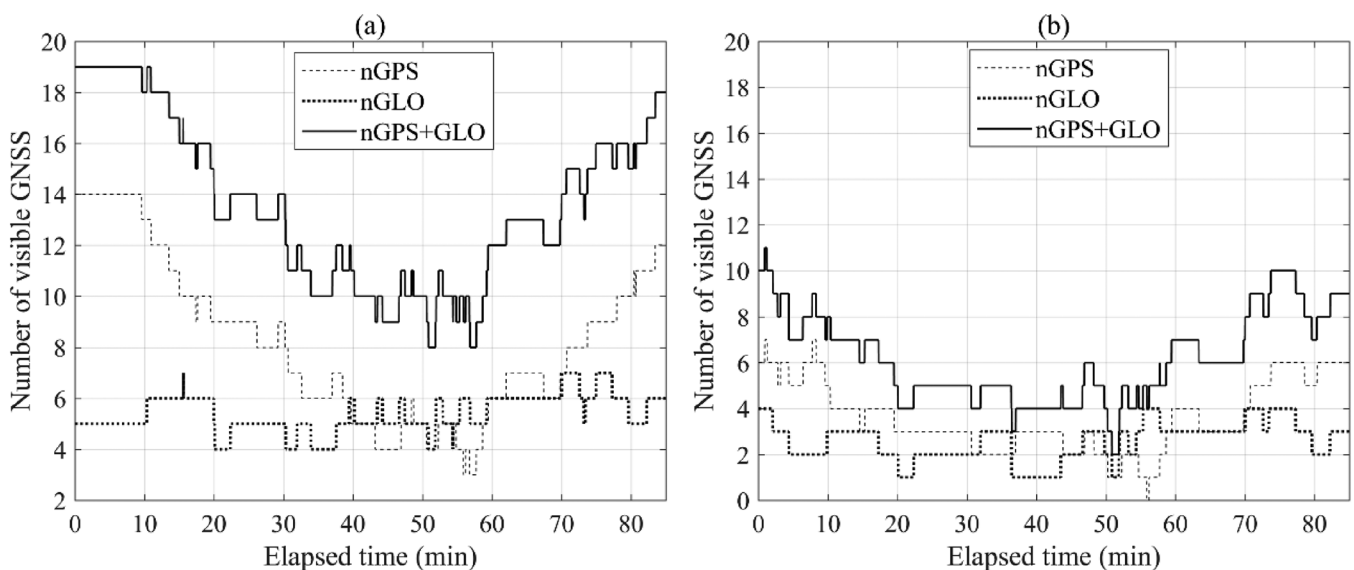


FIGURE 4 Number of common GNSS signals (nGPS: number of GPS; nGLO: number of GLONASS) when the GNSS antennas of two CubeSats (a) point the same direction compared to (b) being pointed with orthogonal direction

maintain each receiver for 175 min and 180 min. Note that the GNSS receiver is necessary only for the AFFP, and the operation phase changes either to the AFFP or DRSKP. In the case of the ISL, Timon transmitted the received GNSS data to Pumbaa once every 5 s.

3 | RELATIVE NAVIGATION METHODOLOGY FOR CANYVAL-C

In this study, an AKF is proposed for the precise relative navigation used by an orbit control system. The term *adaptive* implies that the filter-related parameters are automatically determined during the estimation, rather than by experience-based parameter tuning. This section briefly describes the AKF algorithm and defines the CANYVAL-C navigation problem.

3.1 | Adaptive Kalman filter

The Kalman filter is composed of two steps: prediction and update (Tapley et al., 2004). Starting with an initial guess for the solve-for parameters and covariance matrix, the measurement is predicted by the system model that combines dynamics and observation models. When the measurement data are acquired, the innovation and the Kalman gain are evaluated, and the solve-for parameters are updated. The AKF updates the dynamic noise covariance (Q_i) and the measurement noise covariances (R_i) based on the innovation and residual, while the EKF considers them constants. Figure 5 shows the flows of EKF and AKF as well as the corresponding mathematical details.

In the prediction step, the solve-for parameters and covariance matrix are propagated by employing the dynamics model (f) to the observation time, and the observation model (h) is employed to predict the measurement (y_i^-):

$$X_i^- = f(X_{i-1}^+, t_i),$$

$$P_i^- = \Phi_{i-1,i} P_{i-1}^+ \Phi_{i-1,i}^T + Q \quad \left(\Phi_{i-1,i} = \frac{\partial f_i}{\partial X_{i-1}} \right) \quad (1)$$

$$y_i^- = h(X_i^-) \quad (2)$$

Here, X_i and P_i are the solved vector and covariance matrix at time t_i , respectively, $\Phi_{i-1,i}$ is the state transition matrix from t_{i-1} to t_i , the superscripts - and + indicate predicted and updated values, respectively, and Q is the dynamic noise covariance matrix. When the measurement data (Y) are obtained, the measurement innovation (ΔY_i^-)

is evaluated by comparing the predicted and actual measurements. The Kalman gain (K_i) is also computed using the predicted covariance, sensitivity matrix (H_i), and measurement noise covariances (R):

$$\Delta Y_i^- = Y_i - y_i^- \quad (3)$$

$$K_i = P_i^- H_i^T (H_i P_i^- H_i + R)^{-1} \quad (4)$$

Subsequently, the solve-for vector and covariance matrix are updated. This process is repeated for each observation data point in the case of the EKF:

$$X_i^+ = X_i^- + K_i \Delta Y_i^-, \quad P_i^+ = P_i^- - K_i H_i P_i^- \quad (5)$$

Although EKF is a simple and efficient estimator, it requires an empirical tuning process for the dynamic and measurement noise covariances (Q , R) that have a major impact on the estimation performance. AKF updates them during the estimation using various methods, such as covariance matching. In this research, innovation- and residual-based covariance matching is employed with a dynamic noise scaling method (Akhlaghi et al., 2018; Almagbale et al., 2010). A detailed mathematical process is described.

First, the residual (ΔY_i^+) is computed:

$$\Delta Y_i^+ = Y_i - y_i^+, \quad y_i^+ = h(X_i^+) \quad (6)$$

The measurement noise covariance (R) is estimated by residual-based matching, and the innovation-based dynamic noise covariance (Q'_i) is matched. A forgetting factor (α) is adopted to assign the weights to previous and new estimates by setting $0 \leq \alpha \leq 1$, where a larger value yields a smaller variation in the estimation and takes a longer time to converge (Akhlaghi et al., 2018):

$$R_i = \alpha R_{i-1} + (1 - \alpha) \Delta Y_i^+ (K \Delta Y_i^+)^T \quad (7)$$

$$Q'_i = \alpha Q_{i-1} + (1 - \alpha) K \Delta Y_i^- (K \Delta Y_i^-)^T \quad (8)$$

In the study by Almagbale et al. (2010), the dynamic noise covariance was scaled with a scalar factor (β'_i) as follows:

$$Q_i = \sqrt{\beta'_i} Q_{i-1},$$

$$\beta'_i = \frac{\text{trace} \left(H_i \left(\Phi_{i-1,i} P_{i-1}^+ \Phi_{i-1,i}^T + Q'_i \right) H_i^T \right)}{\text{trace} \left(H_i \left(\Phi_{i-1,i} P_{i-1}^+ \Phi_{i-1,i}^T + Q_{i-1} \right) H_i^T \right)} \quad (9)$$

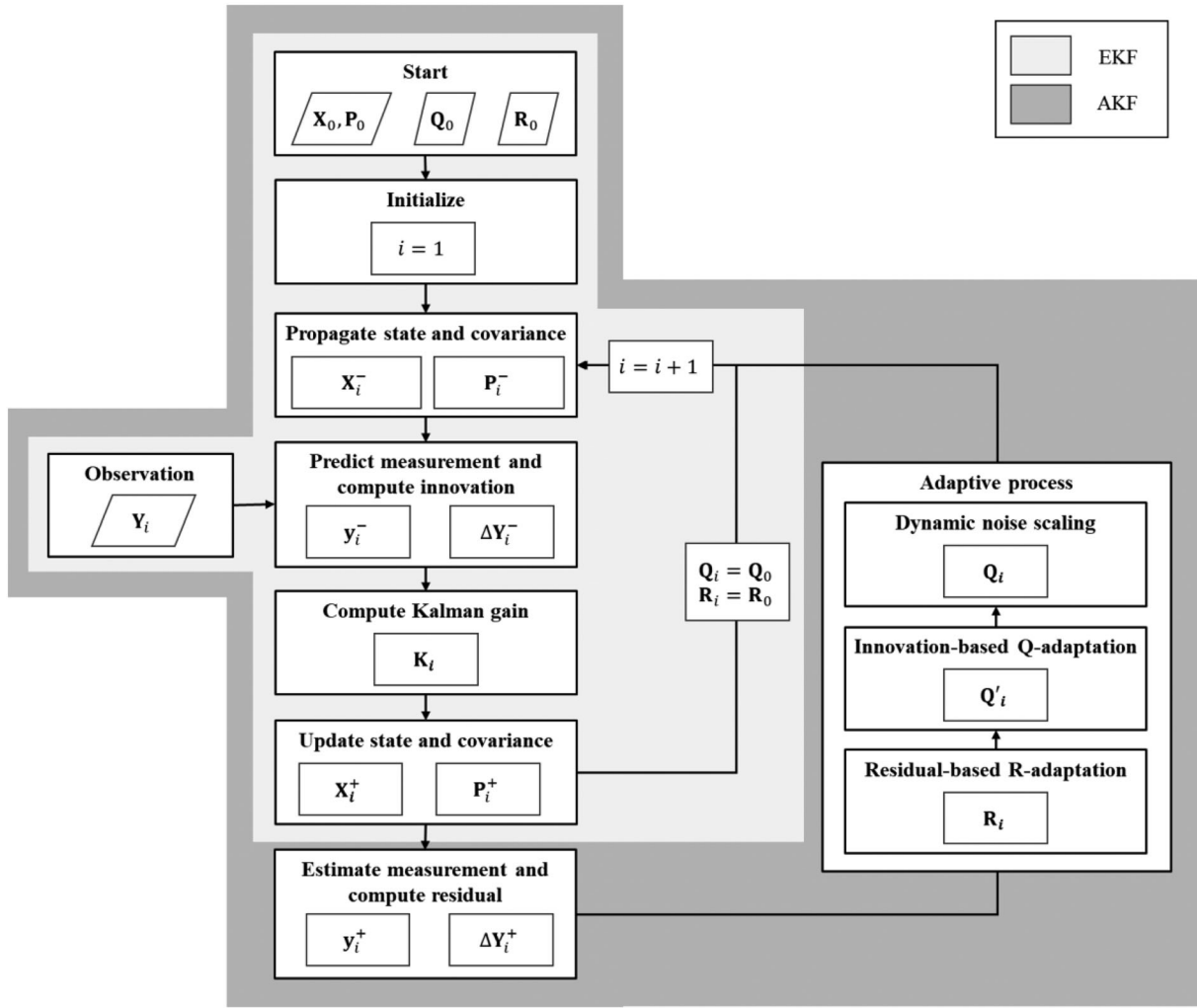


FIGURE 5 Flowchart of the extended and adaptive Kalman filtering processes

In the current research, the scaling method was modified to use a vector with the same dimension as the solve-for vector. It can scale each element of the dynamic noise covariance that makes the covariance more realistic:

$$q_{i,j} = \sqrt{\beta_j} q_{i-1,j}, \quad \beta_i = \text{diag} \left(\frac{\Phi_{i-1,i} P_{i-1}^+ \Phi_{i-1,i}^T + Q'_i}{\Phi_{i-1,i} P_{i-1}^+ \Phi_{i-1,i}^T + Q_{i-1}} \right) \quad (10)$$

Here, $q_{i,j}$ and β_j are the j -th components of Q_i and β_i , respectively.

3.2 | CANYVAL-C relative navigation problem

In this section, the CANYVAL-C relative navigation problem is stated, and the dynamics and GNSS measurement

models are defined. The solve-for vector is established as follows, with subscripts 1 and 2 indicating Timon and Pumbaa, respectively:

$$X = [x_2, \Delta x_{21}, b_2, \dot{b}_2, \Delta b_{21}, \dot{\Delta b}_{21}, \Delta N] \quad (11)$$

where x_2 denotes the absolute position and velocity of Pumbaa, Δx_{21} denotes the relative position and velocity of Pumbaa with respect to Timon, b_2 and \dot{b}_2 are the clock bias and clock bias ratio of Pumbaa, respectively, Δb_{21} and $\dot{\Delta b}_{21}$ are the relative clock bias and clock bias ratio of Pumbaa with respect to Timon, respectively, and ΔN is the difference in the ambiguities of the carrier phase.

Both absolute and relative positions and velocities are defined in the WGS84 coordinate system, which is an Earth-Centered Earth-Fixed (ECEF) coordinate system used by the GNSS. The absolute position and velocity of Timon is not directly estimated but is indirectly computed using the estimation of the absolute and the relative states of Pumbaa.

The dynamics model f contains absolute (f_{abs}) and relative acceleration affecting the CubeSats, and the clock bias drift (f_{clc}), while ambiguity-related terms are maintained constant:

$$f = \begin{bmatrix} f_{abs}(x_2) \\ f_{abs}(x_2) - f_{abs}(x_1) \\ f_{clc}(b_2, \dot{b}_2) \\ f_{clc}(b_2 - b_1, \dot{b}_2 - \dot{b}_1) \\ 0_n \end{bmatrix} \quad (12)$$

where n is the total number of GNSS observations. The relative acceleration is computed by subtracting each absolute acceleration defined in the ECEF coordinates, and the clock bias drift is a simple linear model.

$$f_{abs} = \mu \frac{r}{\|r\|^3} + f_p(r) - 2w_{\oplus} \times v - w_{\oplus} \times r + \vec{u} \quad (13)$$

$$f_{clc} = b + \dot{b}t \quad (14)$$

where r and v are the absolute position and velocity vector in ECEF coordinates, respectively, μ is the gravitational parameter, f_p represents a perturbation model simplified to contain J2 perturbations only, w_{\oplus} is the Earth's rotation vector, and \vec{u} is the thrust for orbit maneuvers.

There are two types of GNSS observables (Cai & Gao, 2007): pseudo-range (P_i^s) and carrier phase (Φ_i^s):

$$P_i^s = \rho_i^s + c(b_i - b^s) + \Delta\rho_{trop} + \Delta\rho_{ion} + \Delta\rho_{multi} + \varepsilon_p \quad (15)$$

$$\Phi_i^s = \rho_i^s + c(b_i - b^s) + \Delta\rho_{trop} - \Delta\rho_{ion} + \Delta\rho_{multi} + \lambda N + \varepsilon_{\Phi} \quad (16)$$

where the subscript i and superscript s indicate the receiver and GNSS satellite, respectively, ρ is the geometric range between the GNSS satellite and receiver, b is the clock bias, c is the speed of light, $\Delta\rho_{trop}$ and $\Delta\rho_{ion}$ are the tropospheric and ionospheric delays, respectively, $\Delta\rho_{multi}$ is the multipath effect, λ is the wavelength of the signal, N is an ambiguity, and ε is the measured noise.

Among the error sources, the clock bias of the GNSS satellite can be compensated by the navigation message. The atmosphere-related delays that have considerable effects on the measurement, however, require complicated models or multifrequency measurements for correction. These are improper to the CANYVAL-C mission which has a restricted computational budget and a single-frequency GNSS receiver. For this reason, CANYVAL-C employs three types of GNSS measurements with simplified measurement models: pseudo-range of the Pumbaa (2U CubeSat), and differences of pseudo-range and carrier phase between the two CubeSats.

The measurement model is given by:

$$h = \begin{bmatrix} P_i^2 \\ P_i^2 - P_i^1 \\ \Phi_i^1 - \Phi_i^1 \end{bmatrix} = \begin{bmatrix} (\|r_2 - r_i^s\| + c(b_2 - b_i^{GNSS}))_{i=1,\dots,n} \\ (\|r_2 - r_i^s\| - \|r_1 - r_i^s\| + c\Delta b_{21})_{i=1,\dots,n} \\ (\|r_2 - r_i^s\| - \|r_1 - r_i^s\| + c\Delta b_{21} + \lambda_i \Delta N_i)_{i=1,\dots,n} \end{bmatrix} \quad (17)$$

where r_1 and r_2 are the position vectors of Timon (1U CubeSat) and Pumbaa (2U CubeSat), and r_i^s is a position vector of the i -th GNSS satellite. In the case of the pseudo-range of Pumbaa, the atmospheric-related correction model and the multipath effects are excluded for simplification. For the other measurements, all error sources are canceled through the subtraction, and only the difference between the clock bias and ambiguity terms remain. Note that the coordinate and time transform algorithms were embedded onboard for matching the systems of GPS and GLONASS (Subirana et al., 2013).

The dynamics model (f) and measurement model (h) defined in this section are identically employed in both onboard EKF and AKF in the ground station. Initially, real-time estimation using onboard EKF was conducted with empirically tuned parameters. The downlink data from the CubeSats included the received GNSS data, orbit solution of the receiver, and the relative navigation results.

After each communication between the CubeSat and the ground station, the relative navigation results were analyzed by comparing with two references: First, the onboard relative navigation results were compared to the downloaded orbit solution computed by the onboard receiver. Second, the results were compared to the subtraction of the absolute states of the CubeSats determined by the Flight Dynamics System (FDS) using GNSS data. If analyses of the differences and covariances yield unreasonable results, e.g., the differences exceed 4σ boundary of the covariance, the adaptive process would be executed using the received GNSS data, and the adaptively determined parameters would be uploaded to the CubeSats to be employed to onboard navigation.

4 | HARDWARE-IN-THE-LOOP SIMULATIONS

This section details the verification of the relative navigation algorithm based on HILS. The system for HILS is composed of a signal generator, flight control system, remote control system, signal monitoring system, and receiver

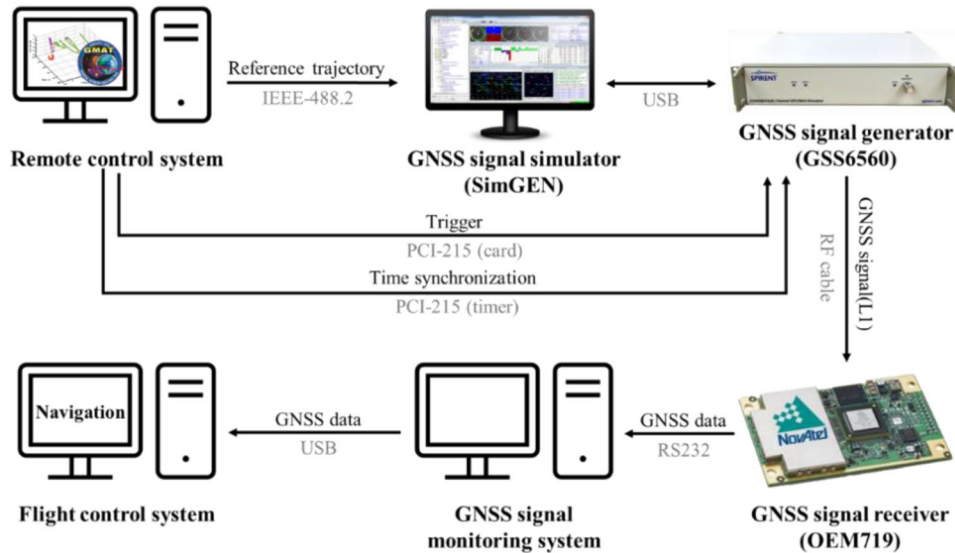


FIGURE 6 Data interface and flow of the Hardware-in-the-Loop Simulation (HILS) system [Color figure can be viewed in the online issue, which is available at wileyonlinelibrary.com and www.ion.org]

(Park et al., 2010). The signal generator is a Spirent Communications' GSS 6560 simulator that consists of a Radio Frequency (RF) signal generator and a personal computer for operation. It simulates the GNSS signal in L1 frequency, and the transmitted signal can be received through the RF cable or antenna.

The flight control system contains both navigation algorithms based on the GNSS data and control algorithm, and the remote control system provides a controlled trajectory of the satellite to the signal generator in real time that enables closed-loop simulation. In this research, however, the remote control system transfers a reference trajectory based on the orbit control scenario, and the flight control system employs only the navigation algorithm. The receiver was an OEM719 (the same as that of the cube), and the corresponding signal monitoring system was employed.

Figure 6 presents the data interface and flow of the HILS system, where the gray and black colors near the arrows indicate interface and data, respectively. The generated pseudo-tracking data and the simulation conditions are explained in Section 4.1, and the navigation results are shown in Section 4.2.

4.1 | Simulation scenarios

Based on four orbit control scenarios of CANYVAL-C for three RDV modes (RDV-1, RDV-2, and RDV-3) and one IAH mode, the reference trajectories were generated for the two CubeSats in a Sun-synchronous orbit at an altitude of 500 km. Note that the altitude is different from the real

TABLE 2 Physical properties of the CubeSats and dynamical circumstances used to generate trajectories for GNSS tracking data

Property	1U	2U
Mass (kg)	0.9618	2.3754
Mean area (m ²)	0.0114	0.0321
Drag coefficient	2.2	
Solar Radiation Pressure (SRP) coefficient	1.0	
Epoch date (UTC)	1 Jun 2020 00:00:00 (RDV) 1 Sep 2020 00:00:00 (IAH)	
Gravity model	EGM96 70 × 70	
3 rd body perturbation	Sun, Moon, Jupiter	
Atmospheric model	Exponential atmosphere	
SRP model	Sphere	
Uncertainty of thrust direction (°)	1	
Uncertainty of thrust magnitude (%)	5	
Propagator	Runge–Kutta 78	

one (525 km) because, for practicality, the orbit for the simulation was approximately designated before the final orbit was decided. The trajectories were generated considering the physical and dynamical conditions (Table 2) to imply the real dynamical circumstance, whereas the onboard navigation employs the simplified dynamics model (Section 3.2).

Each scenario was generated with different orbital states and control profiles. Figure 7 shows the control profiles of the scenarios in Earth-centered inertial coordinates. They

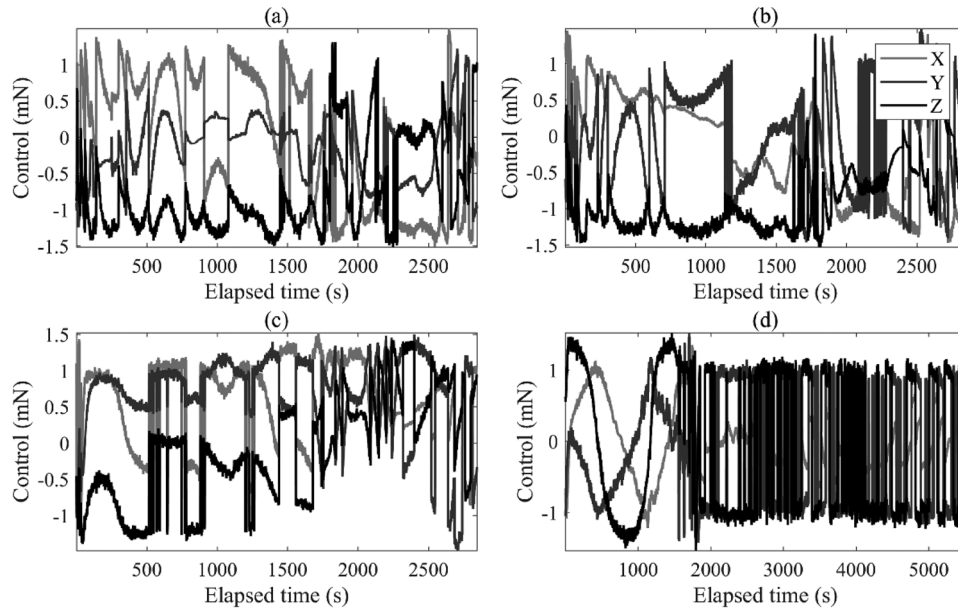


FIGURE 7 Control profiles during (a) RDV-1, (b) RDV-2, (c) RDV-3, and (d) IAH modes

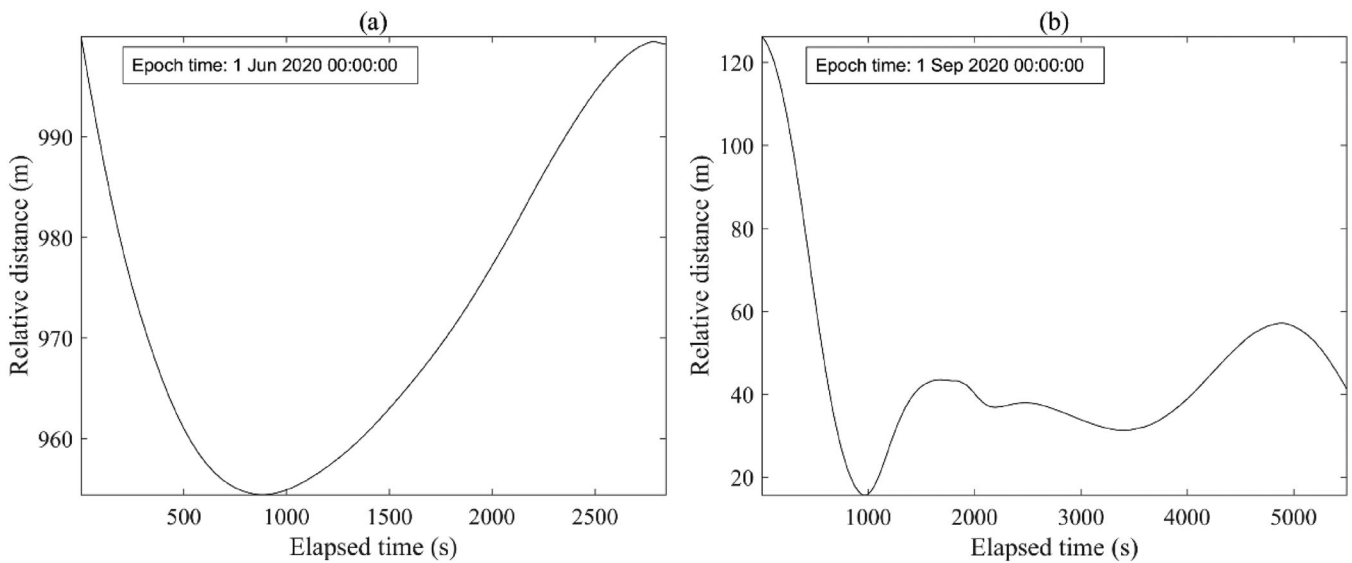


FIGURE 8 Distances between two CubeSats and control profiles during (a) RDV and (b) IAH modes

were computed considering the constraint of maximum thrust of 1 mN and provided for the navigation algorithm as feedback involving a magnitude error of 5 % (Section 3.2). Note that the distances between the CubeSats were maintained at approximately 40 m for 200 s in the IAH mode and values < 1 km in the RDV modes as shown by Figure 8.

The pseudo-GNSS signals of both the GPS and GLONASS were generated by SimGEN and received by OEM719. Figure 9 indicates the number of common signals from the GPS and GLONASS, considering the constraints of the GNSS antenna direction described in Section 2.2.

Three scenarios were differently employed. The RDV-1 and IAH mode scenarios were employed for both the adaptive process and onboard navigation, and RDV-2 and RDV-3 mode scenarios were applied only to onboard navigation.

4.2 | Results

This section compares and analyzes the estimated results of the classical EKF and AKF. For the EKF, the dynamic

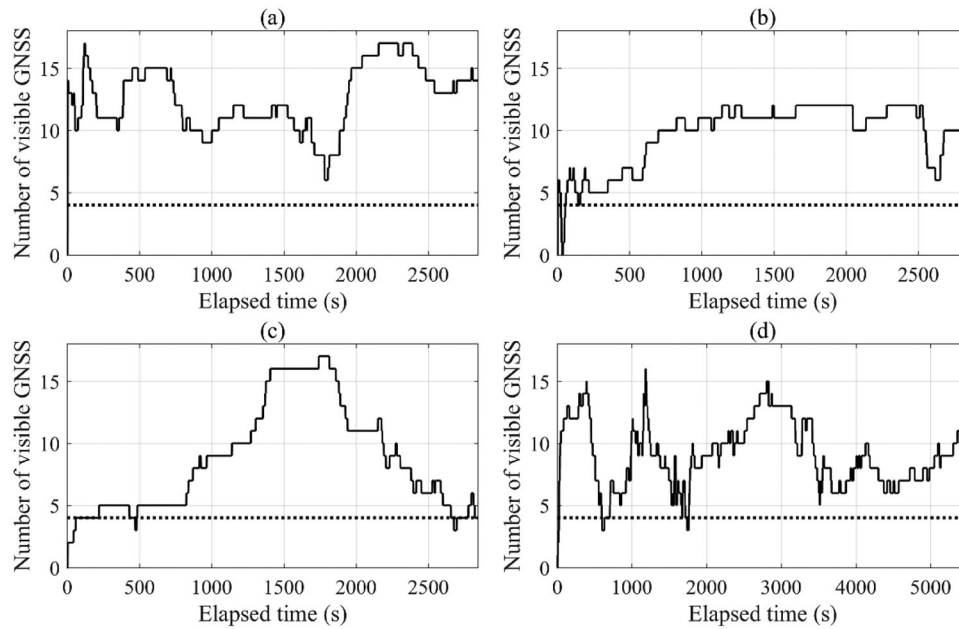


FIGURE 9 Number of common signals for the relative navigation during (a) RDV-1, (b) RDV-2, (c) RDV-3, and (d) IAH modes

and measurement noise covariances as well as the tuning parameters should be experimentally designated. The parameters significantly influence performance, whereas tuning is not as straightforward. In fact, tuning is complicated, especially for space missions because realistic circumstances cannot be known before the actual launch operations.

In this simulation, EKF started with the empirically tuned parameters based on numerous numerical simulations, while AKF employed arbitrary parameters because they were adapted to the actual circumstance during the estimation. The forgetting factor (α) defined in Section 3.1 was set to 0.8, which is a relatively large value used to prevent temporary variation and lead to stable estimation. For both estimators, the a priori errors for the absolute states were assumed as random Gaussian errors of 50 m for the position and 0.05 m/s for the velocity in each axis. Note that all errors were evaluated by comparing the reference trajectory, as described in Section 4.1, and analyzed based on definitions in the ECEF coordinates.

The relative position errors of both estimators for the IAH mode are presented in Figure 10. The errors of the EKF converged to approximately a few tens of centimeters within a timeframe of 50 s, while the error covariance did not correspond to the error. This implies that the system characteristics were not reflected in the noise covariances that were used to compute the error covariance.

Conversely, in the case of the AKF, this error converged to 1 cm after 2000 s, which is smaller than the error of the EKF. The converged error level was in accordance with that of a previous study (Busse et al., 2003) that used the

absolute state from the GNSS receiver and focused on the estimation of relative parameters only, such as the relative state and differences in the clock bias.

Unlike the case of the EKF, the uncertainty boundaries evaluated by the error covariance also described actual estimation errors. Compared with the empirically tuned parameters, it was confirmed that the adaptively determined parameters depicted the actual system and provided a realistic error covariance. The error covariance provides a reliable error bound covering the actual errors which is significant because, in practice, only a matrix is used to assess the estimation accuracy.

Figure 11 shows the changes in each element of the measurement noise covariance R and dynamic noise covariance Q during the adaptive process (with AKF): elements of measurement noise covariance for pseudo-range (PR), relative pseudo-range (rPR), and relative carrier phase (rCP), elements of dynamic noise covariance for absolute position and velocity (Q_{Pos} , Q_{Vel}), and relative position and velocity (Q_{RelPos} , Q_{RelVel}).

The measurement noise covariance immediately converged, and the dynamic noise covariance converged at approximately 2,000 s after its onset. Both the relative position errors of AKF (Figure 9, lower graphs) and the changes in the dynamic noise covariances (Figure 10) required approximately 2,000 s. This implies that the dynamic noise covariance significantly affects the navigation performance, emphasizing the importance of the exact determination of the covariance. The adaptive process (AKF) can robustly determine the exact covariance values starting with arbitrary initial guesses. This can reduce

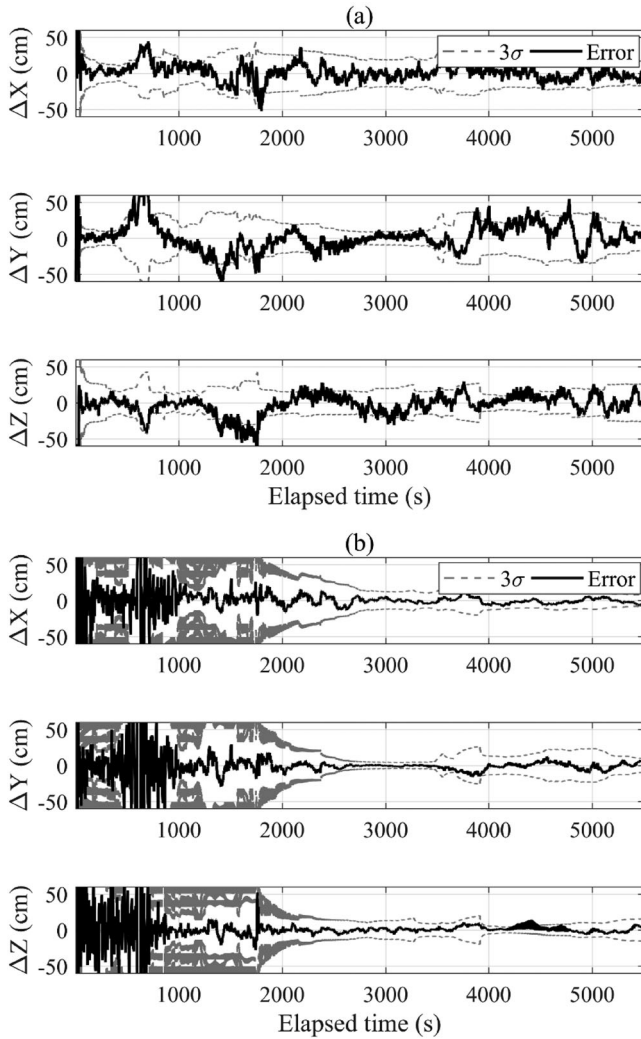


FIGURE 10 Relative position error of (a) the Extended Kalman Filter (EKF) and (b) Adaptive Kalman Filter (AKF) in IAH mode

the time and effort required to identify appropriate initial guesses.

Assuming the practical operation of CANYVAL-C, wherein the adaptively determined parameters (Q , R) are uploaded and employed to the CubeSats, relative navigation was conducted onboard using an EKF with the determined tuning parameters. The adaptively determined parameters in the IAH mode were applied to the onboard relative navigation algorithm (EKF) for (1) the same IAH mode and (2) the three different RDV modes to examine the applicability and consistency of the parameters. The mean values of the tuning parameters at the last 1,000 s (after the convergence) were considered as adaptively determined values.

The parameters determined through the AKF were employed for the relative navigation in the same IAH mode scenario. Figure 12 shows the measurement residuals and

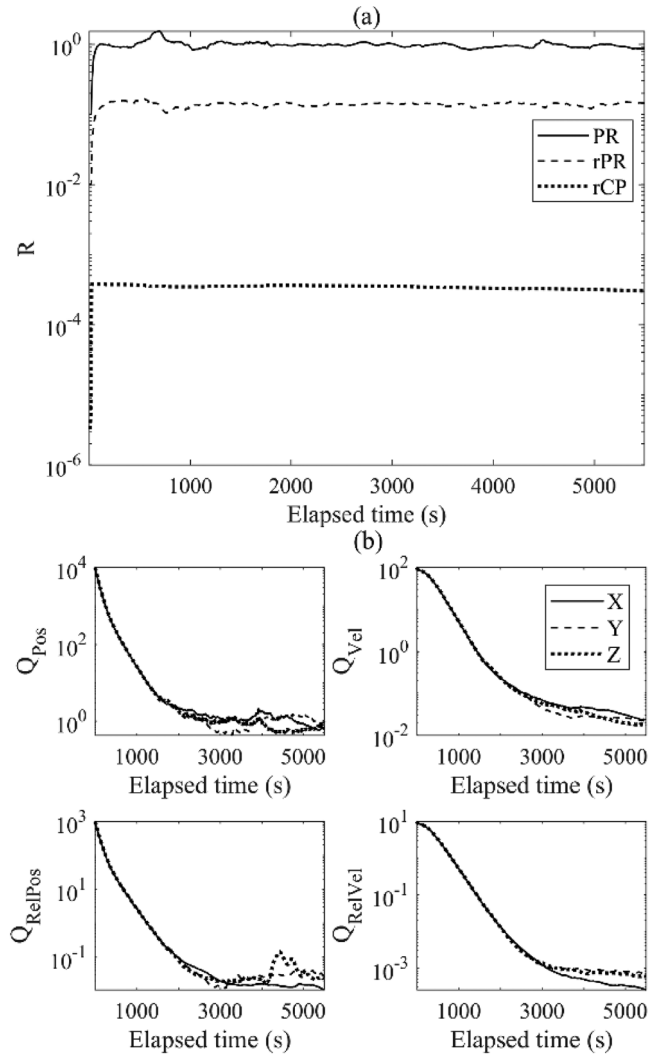


FIGURE 11 Changes of (a) measurement noise covariance and (b) dynamic noise covariance during the adaptive process

relative position errors of the EKF. The residuals and positional errors converged to a steady level within 50 s, and the covariance matrix provided the proper uncertainty boundary representing the error.

Table 3 shows the Root-Mean-Square (RMS) values of the relative position errors using an EKF with empirically tuned and adaptively determined parameters, wherein the accuracy improved by 45%–71% for each axis and by 61% in 3D for the adaptive case.

Although both cases satisfied the CANYVAL-C mission requirement for relative position, the absolute position errors in the case of the empirically tuned parameters did not satisfy the requirement by exceeding 50 m in 3D, and the error covariance did not coincide with the errors. Conversely, the adaptively determined parameters provided an absolute position error of less than 10 m for each axis, and the error covariance matched the errors (Figure 13).

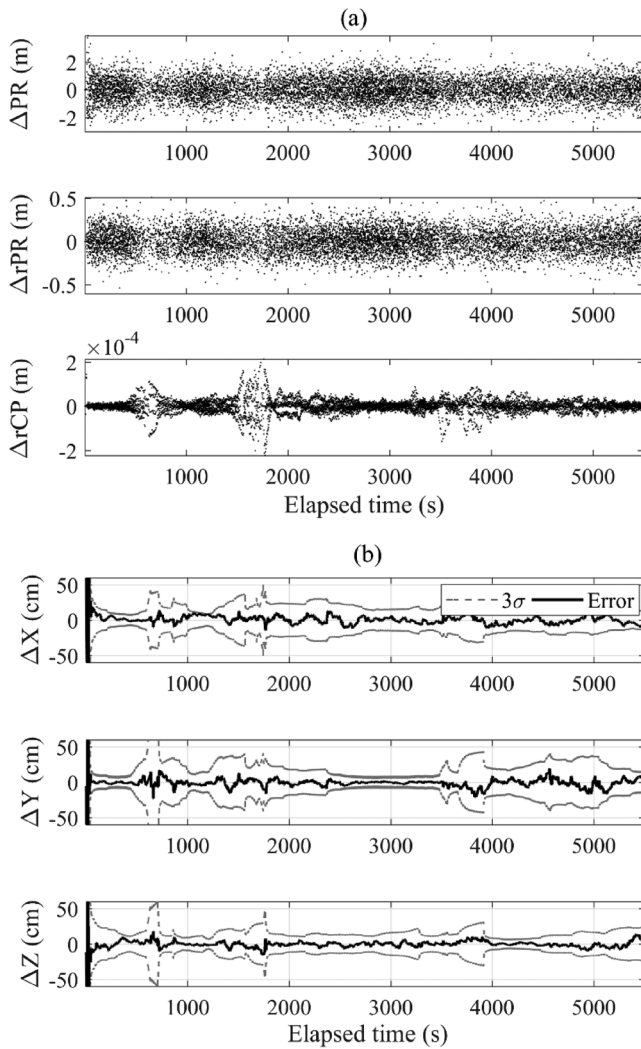


FIGURE 12 (a) Measurement residuals and (b) relative position errors of EKF for IAH mode with the adaptively determined parameters in IAH mode

TABLE 3 RMS values of relative position errors of EKF for the IAH mode using empirically tuned and adaptively determined parameters

Tuning method	X (cm)	Y (cm)	Z (cm)	3D (cm)
Empirical	11.3801	19.0551	14.3376	26.4230
Adaptive	6.2275	7.4983	4.4482	10.7141

In terms of reliability, an estimator must determine all solve-for parameters, even if strict requirements are set for only a part of these parameters. It was verified that the adaptive process can properly determine all the elements in the dynamic and measurement noise covariances, thus making a stable estimation. This is especially valuable in the case of the high dimensionality of the solve-for parameters wherein the empirical tuning process is more complicated.

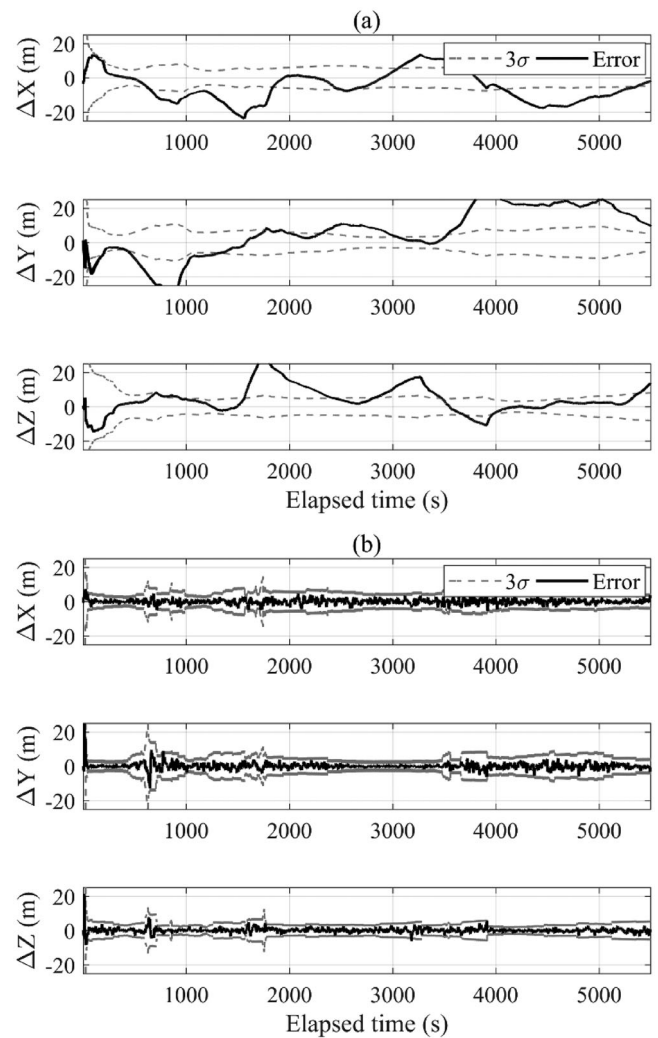


FIGURE 13 Absolute position errors of EKF for IAH mode with (a) the empirically tuned and (b) the adaptively determined parameters in IAH mode

The onboard relative navigation using EKF was conducted for three RDV scenarios with the tuning parameters that were adaptively determined according to the IAH mode scenario. Figure 14 and Table 4 show the relative position errors and RMS error values in each case that satisfied the mission requirement.

Compared to the RDV-1 case, the RDV-2 and RDV-3 cases took more time for convergence and had increased errors at the end time. This was attributed to the decreasing number of common GNSS signals, which reduced the navigation accuracy. The RDV-2 and RDV-3 had fewer than 10 signals at the start and end, whereas the RDV-1 had more than 10 signals for almost the entire duration. After the convergence occurred at 700 s, the RMS errors were 6.8 and 14 cm for RDV-2 and RDV-3 modes, respectively. This implies that the adaptively determined parameters represent the system well, regardless of the tracking data

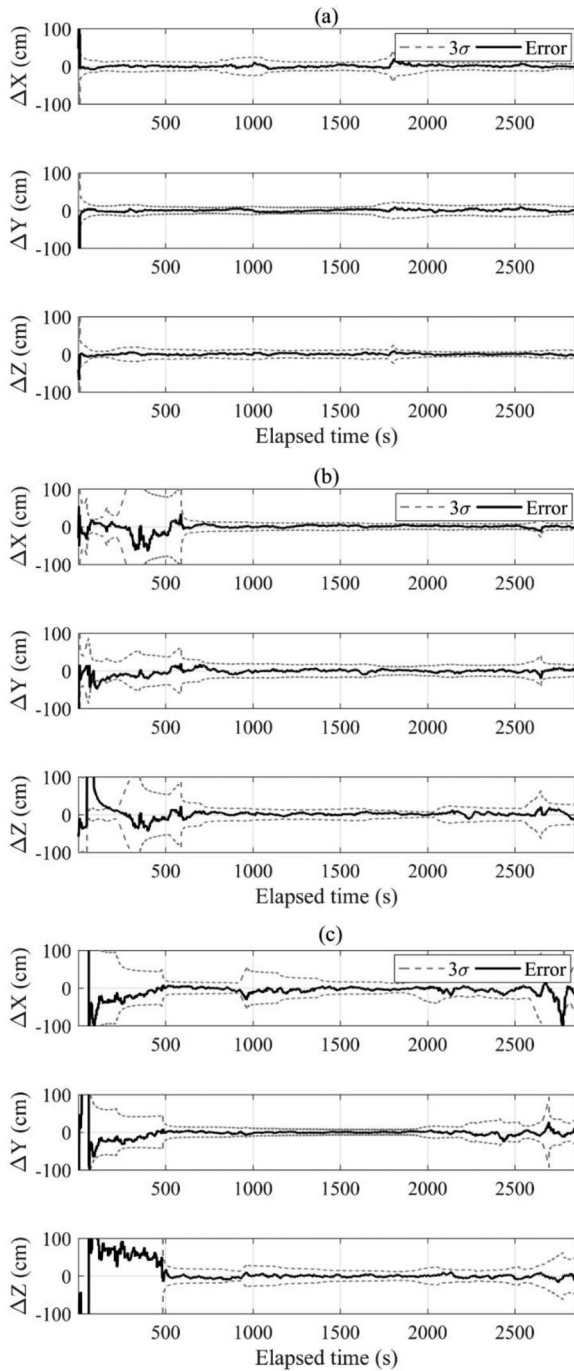


FIGURE 14 Relative position errors of (a) RDV-1, (b) RDV-2, and (c) RDV-3 mode scenarios with adaptively determined tuning parameters in IAH mode

TABLE 4 RMS of relative position errors of EKF for three RDV modes using adaptively determined parameters in IAH mode

Applied scenario	X (cm)	Y (cm)	Z (cm)	3D (cm)
RDV-1	3.3993	2.7706	2.2121	4.9117
RDV-2	10.6763	8.3295	21.3251	25.2611
RDV-3	17.1743	9.9453	27.7249	34.0960

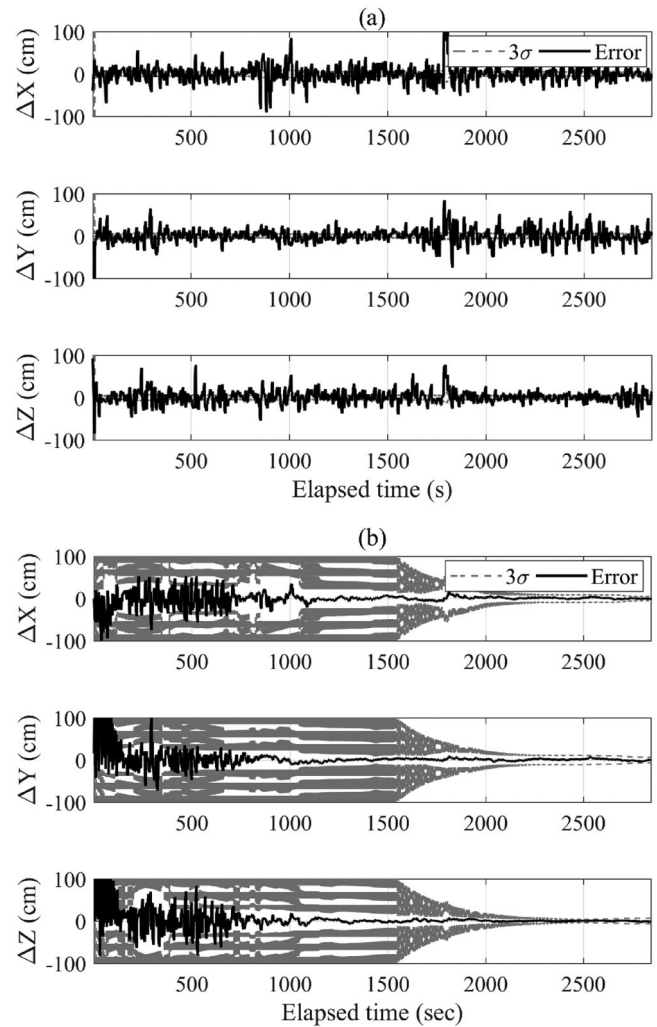


FIGURE 15 Relative position errors of (a) EKF and (b) AKF in RDV-1 mode

and control scenarios. Therefore, this confirms the reliability and consistency of the parameters. The proposed technique was verified to be capable of providing reliable navigation performance without imposing an additional computational burden on the onboard CubeSat computer.

In the RDV-1 mode scenario, similar analyses as those in the IAH mode were conducted. After the adaptive process for the RDV-1 scenario, the adaptively determined parameters were applied for the onboard navigation test using EKF (1) to the same RDV-1 scenario and (2) to different scenarios. All RDV scenarios had the same epoch time, while the epoch time of the IAH scenario was three months later than that of the RDV.

As in the case of the IAH mode, the relative position errors of the EKF with empirically tuned parameters rapidly converged to a steady state, but the error covariance did not depict the errors. The errors of AKF satisfied the requirement after 1,500 s with the corresponding error covariance (Figure 15). Using the adaptively determined

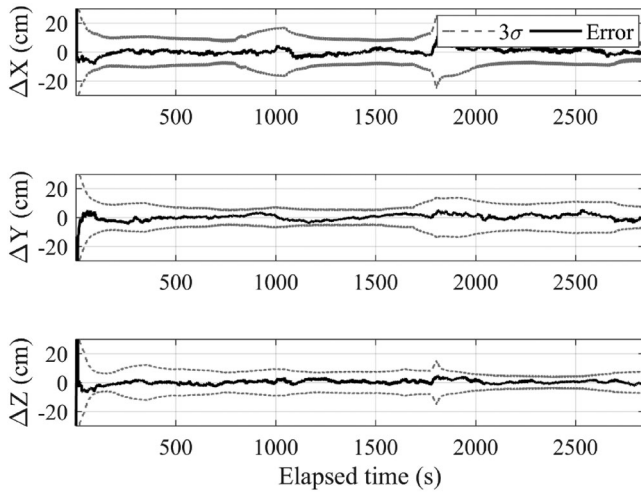


FIGURE 16 Relative position errors of EKF for RDV-1 mode with the adaptively determined parameters in RDV-1 mode

parameters, EKF converged within 50 s, and the accuracy was improved to approximately 7 cm (3σ) on each axis for the same RDV-1 scenario (Figure 16).

Unlike the case with the empirically tuned parameters, the adaptively determined parameters provided the error covariance that closely matched the actual estimation errors. This achieved a practical analysis of the estimation accuracy. For the IAH, RDV-2, and RDV-3 scenarios, the parameters were applied, and the relative position errors converged to 10 cm (3σ) for each axis within a period of 50 s in the IAH mode and within a period of 500 s in the RDV modes (Figure 17).

Table 5 shows the RMS of the relative errors that satisfied the mission requirement of the relative position in all cases. Similar to the results using the adaptively determined parameters in IAH mode, the errors were large at the end time, and the time required for convergence was relatively long in the cases of the RDV-2 and RDV-3. The RMS errors after convergence were 4.3 and 9.6 for each mode.

Through the analyses of four different scenarios, the distinct advantages of AKF were proven, and the operation technique for CANYVAL-C was verified. The adaptive process robustly identified the tuning parameters regardless of the a priori states and initial guesses for the parameters. This effectively reduced the time and effort required to guess the proper initial value or empirically tune the parameters.

The determined parameters reliably estimated all the state parameters and described the actual system accurately. The error covariance associated with the use of the parameters indicates the actual error and led to a realistic analysis in practical situations. Because the operation technique was designated to execute the process in the ground

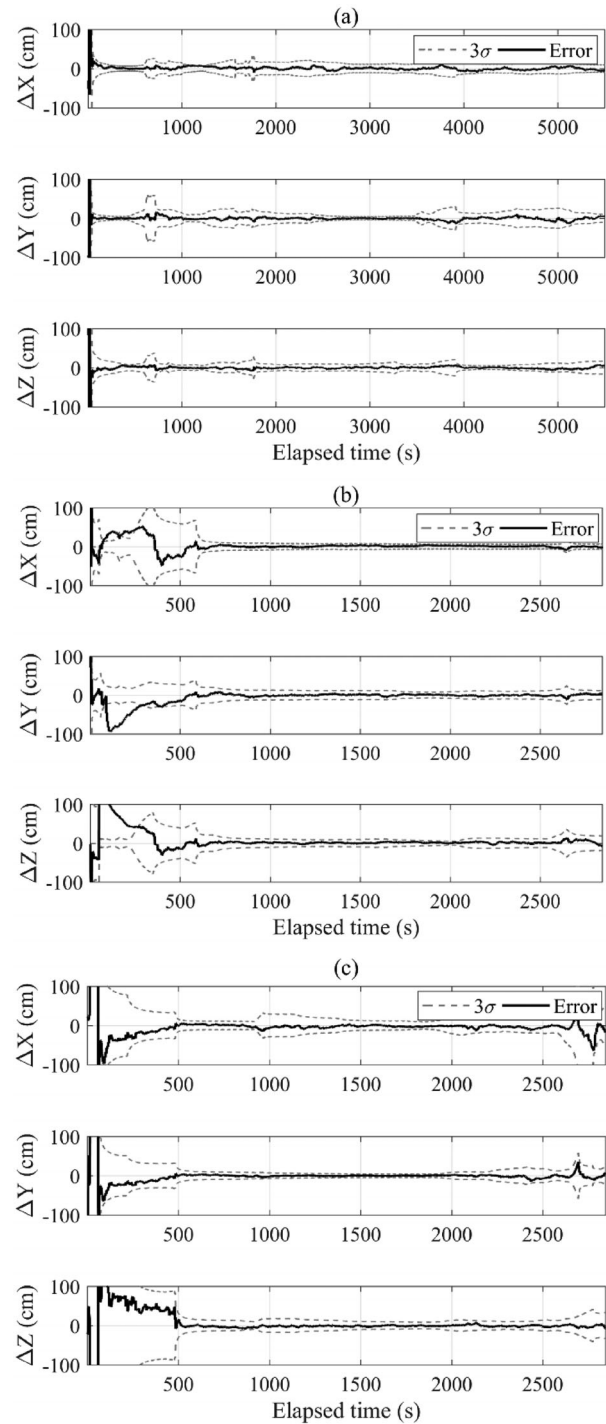


FIGURE 17 Relative position errors of EKF for (a) IAH, (b) RDV-2, and (c) RDV-3 modes with adaptively determined tuning parameters in the RDV-1 mode

station, no additional computational burden was induced to the onboard computer of the CubeSat.

The practical applicability of the technique for a time-separated environment was proven, whereby onboard relative navigation was conducted with parameters adaptively determined based on actual GNSS data that were received

TABLE 5 RMS of relative position errors of EKF for IAH and the three RDV modes using adaptively determined parameters in the RDV-1 mode

Applied scenario	X (cm)	Y (cm)	Z (cm)	3D (cm)
IAH	3.5252	3.6836	2.7501	5.7930
RDV-1	2.5505	1.8583	1.6038	3.5398
RDV-2	18.4737	20.6161	30.7802	41.3971
RDV-3	16.4849	10.2361	28.4614	34.4467

from the CubeSat several hours earlier. In practical operation after the launch of the CANYVAL-C, the relative navigation results were validated by comparing both the downloaded orbit solution computed by the onboard receiver and the determined orbit states by FDS. If the results seem not to be reasonable after analyzing the differences and covariances or if considerable system changes occur, the adaptive process would be conducted and the adaptively determined parameters would be uploaded to improve performance.

5 | CONCLUSIONS

This study developed a relative navigation algorithm that employs EKF and AKF for CANYVAL-C with mission constraints, proposed an operation technique for precise and reliable relative navigation, and verified its performance using HILS. The operation technique ensured that the ground station adaptively determines the tuning parameters by a modified AKF and uploads them onboard, and the CubeSats conduct relative navigation by applying the parameters to the EKF.

For the adaptive algorithm, the innovation- and residual-based covariance matching was employed by adding a modified scaling method for the dynamic noise. The method scales each element of the dynamic noise using a scaling parameter having the same dimension as the state vector. In the case of HILS, four scenarios of CANYVAL-C, including the constraints, were employed: the adaptive process took IAH and RDV mode scenarios, and the adaptively determined parameters were applied to all scenarios, including another two RDV mode scenarios, to examine consistency and reliability.


Adopting the adaptively determined parameters, the relative navigation accuracies satisfied the mission requirements in all cases. The results confirmed the robustness of the adaptive process and the practicality and reliability of the estimation with the adaptively determined parameters. The adaptive process provided steady tuning parameters, regardless of the initial guess. This reduced the time and effort required to identify proper initial guesses and

tune parameters. The adaptively determined parameters led to reliable estimation for all solve-for parameters and represented the actual system accurately to lead realistic error analysis using the error covariance. It was verified that use of the proposed operation concept led to reliable real-time relative navigation without imposing an additional computational burden on CubeSat. After the launch of CANYVAL-C scheduled in early 2021, the technique will be applied to practical operations.

ACKNOWLEDGMENTS

Space Basic Technology Development Program through the National Research Foundation (NRF) of Korea funded by the Ministry of Science and ICT of the Republic of Korea (NRF-2017M1A3A3A06085349).

ORCID

Sang-Young Park  <https://orcid.org/0000-0002-1962-4038>

REFERENCES

- Akhlaghi, S., Zhou, N. & Huang, Z. (2018). Adaptive adjustment of noise covariance in Kalman filter for dynamic state estimation. *IEEE Power and Energy Society General Meeting*. <https://doi.org/10.1109/PESGM.2017.8273755>
- Almagbile, A., Wang, J., & Ding, W. (2010). Evaluating the performances of adaptive Kalman filter methods in GPS/INS integration. *Journal of Global Positioning Systems*. <https://doi.org/10.5081/jgps.9.1.33>
- Andersen, G., Asmolov, O., Dearborn, M. E., & McHarg, M. G. (2012). FalconSAT-7: a membrane photon sieve CubeSat solar telescope. *Space Telescopes and Instrumentation 2012: Optical, Infrared, and Millimeter Wave*. <https://doi.org/10.1117/12.924250>
- Bonin, G., Roth, N., Armitage, S., Newman, J., Risi, B. & Zee, R. E. (2015). CanX-4 and CanX-5 Precision Formation Flight: Mission Accomplished! Proceedings of the 29th Annual AIAA/USU Conference on Small Satellites. <https://digitalcommons.usu.edu/cgi/viewcontent.cgi?article=3167&context=smallsat>
- Busse, F. D., How, J. P., & Simpson, J. (2003). Demonstration of adaptive extended Kalman filter for low-earth-orbit formation estimation using CDGPS. *NAVIGATION*, 50, 79–93. <https://doi.org/10.1002/j.2161-4296.2003.tb00320.x>
- Cai, C., & Gao, Y. (2007). Precise point positioning using combined GPS and GLONASS observations. *Journal of Global Positioning Systems*, 6, 13–22. <http://citeseerx.ist.psu.edu/viewdoc/download?doi=10.1.1.524.3103&rep=rep1&type=pdf>
- Calhoun, P. C., Novo-Gradac, A. M., & Shah, N. (2018). Spacecraft alignment determination and control for dual spacecraft precision formation flying. *Acta Astronautica*, 153, 349–356. <https://doi.org/10.1016/j.actaastro.2018.02.021>
- Fish, C. S., Swenson, C. M., Crowley, G., Barjatya, A., Neilsen, T., Gunther, J., Azeem, I., Pilinski, M., Wilder, R., Allen, D., Anderson, M., Bingham, B., Bradford, K., Burr, S., Burt, R., Byers, B., Cook, J., Davis, K., Frazier, C., ... Cousins, M. (2014). Design, development, implementation, and on-orbit performance of the dynamic ionosphere cubesat experiment mission. *Space Science Reviews*, 181, 61–120. <https://doi.org/10.1007/s11214-014-0034-x>

- He, X. T., Nan, J., & Zhen, S. Z. (2012). An improved adaptive Sage filter with applications in GEO orbit determination and GPS kinematic positioning. *Science China: Physics, Mechanics and Astronomy*, 55, 892–898. <https://doi.org/10.1007/s11433-012-4659-z>
- Johnston-Lemke, B. & Zee, R. E. (2010). Attitude maneuvering under dynamic path and time constraints for improved GPS coverage of formation-flying nanosatellites. *61st International Astronautical Congress 2010*, IAC 2010.
- Kaaret, P., Zajczyk, A., Larocca, D. M., Ringuette, R., Bluem, J., Fuelberth, W., Gulick, H., Jahoda, K., Johnson, T. E., Kirchner, D. L., Koutroumpa, D., Kuntz, K. D., McCurdy, R., Miles, D. M., Robison, W. T. & Silich, E. M. (2019). Halosat: A cubesat to study the hot galactic halo. In arXiv. <https://doi.org/10.3847/1538-4357/ab4193>
- Kahr, E., Roth, N., Montenbruck, O., Risi, B., & Zee, R. E. (2018). GPS relative navigation for the CanX-4 and CanX-5 formation-flying nanosatellites. *Journal of Spacecraft and Rockets*, 55(6). <https://doi.org/10.2514/1.A34117>
- Karlgard, C. D., & Schaub, H. (2011). Adaptive nonlinear huber-based navigation for rendezvous in elliptical orbit. *Journal of Guidance, Control, and Dynamics*, 34(2). <https://doi.org/10.2514/1.51939>
- Kim, G.-N., Park, S.-Y., Kang, D.-E., Son, J., Lee, T., Jeon, S., Kim, N., & Park, Y.-K. (2019). Development of CubeSats for CANYVAL-C mission in formation flying. *APISAT 2019: Asia Pacific International Symposium on Aerospace Technology* (pp. 813–824). Engineers Australia.
- Klesh, A., Clement, B., Colley, C., Essmiller, J., Forgette, D., Krajewski, J., Marinan, A., Martin-mur, T., Steinkraus, J., Sternberg, D., Werne, T. & Young, B. (2018). MarCO: Early Operations of the First CubeSats to Mars. *32nd Annual AIAA/USU Conference on Small Satellites*. <https://digitalcommons.usu.edu/smallsat/2018/all2018/474>
- Leonard, C. L., Hollister, W. M., & Bergmann, E. V. (1989). Orbital formationkeeping with differential drag. *Journal of Guidance, Control, and Dynamics*, 12(1), 108–113. <https://doi.org/10.2514/3.20374>
- Llorente, J. S., Agenjo, A., Carrascosa, C., De Nequeruela, C., Mestreau-Garreau, A., Cropp, A., & Santovincenzo, A. (2013). PROBA-3: Precise formation flying demonstration mission. *Acta Astronautica*, 82(1), 38–46. <https://doi.org/10.1016/j.actaastro.2012.05.029>
- Morrison, J. M., Jeffrey, H., Gorter, H., Anderson, P., Clark, C., Holmes, A., Feldman, G. C., & Patt, F. S. (2016). SeaHawk: an advanced CubeSat mission for sustained ocean colour monitoring. *Sensors, Systems, and Next-Generation Satellites XX*. <https://doi.org/10.1117/12.2241058>
- Park, J. I., Park, H. E., Park, S. Y., & Choi, K. H. (2010). Hardware-in-the-loop simulations of GPS-based navigation and control for satellite formation flying. *Advances in Space Research*, 46(11), 1451–1465. <https://doi.org/10.1016/j.asr.2010.08.012>
- Park, J. P., Park, S. Y., Song, Y. B., Kim, G. N., Lee, K., Oh, H. J., Yim, J. C., Lee, E., Hwang, S. H., Kim, S., Choi, K. Y., Lee, D. S., Kwon, S. H., Kim, M. S., Yeo, S. W., Kim, T. H., Lee, S. H., Lee, K. B., Seo, J. W. & Jin, S. . . . (2016). Cubesat development for canyval-X mission. *SpaceOps 2016 Conference*.
- Park, S. Y., Calhoun, P. C., Shah, N. & Williams, T. W. (2014). Orbit design and control of technology validation mission for refractive space telescope in formation flying. *AIAA Guidance, Navigation, and Control Conference*.
- Roscoe, C. W. T., Westphal, J. J., & Mosleh, E. (2018). Overview and GNC design of the CubeSat Proximity Operations Demonstration (CPOD) mission. *Acta Astronautica*, 153, 410–421. <https://doi.org/10.1016/j.actaastro.2018.03.033>
- Shah, N., Calhoun, P., Dennis, B., Krizmanic, J., Shih, A. & Skinner, G. (2013). The Virtual Telescope Demonstration Mission (VTDM). *5th International Conference on Spacecraft Formation Flying Missions and Technologies*. [https://www.semanticscholar.org/paper/THE-VIRTUAL-TELESCOPE-DEMONSTRATION-MISSION-\(-VTDM-Shah-Calhoun/8784b636b6e157e9f0ad90c55d489ce7f4c11400](https://www.semanticscholar.org/paper/THE-VIRTUAL-TELESCOPE-DEMONSTRATION-MISSION-(-VTDM-Shah-Calhoun/8784b636b6e157e9f0ad90c55d489ce7f4c11400)
- Subirana, J., Zornoza, J. M. J., & Hernández Pajares, M. (2013). *GNSS Data Processing Volume I: Fundamentals and Algorithms (ESA TM-23/I; May 2013)*. Noordwijk, Netherlands: ESA Communications, ESTEC. https://gssc.esa.int/navipedia/GNSS_Book/ESA_GNSS-Book_TM-23_Vol_I.pdf
- Tapley, B. D., Schutz, B. E., & Born, G. H. (2004). *Statistical Orbit Determination*. Elsevier Inc. <https://doi.org/10.1016/B978-0-12-683630-1.X5019-X>
- Xiao, Y., Li, L., Chang, J., Wu, K., Liang, G., & Yu, J. (2018). A novel GPS based real time orbit determination using adaptive extended kalman filter. *IEICE Transactions on Fundamentals of Electronics, Communications and Computer Sciences*, E101-A(1), 287–292.

How to cite this article: Lee E, Son J, Park S-Y. Relative navigation technique with constrained GNSS data for formation-flying CubeSat mission, CANYVAL-C. *NAVIGATION*. 2021;68:559–575. <https://doi.org/10.1002/navi.439>